## From First Principles to Quantum Electrodynamics: Pushing the Limits of Theory with the Hydrogen Molecule

Krzysztof Pachucki\*,† and Jacek Komasa\*,‡

†Faculty of Physics, University of Warsaw, Pasteura 5, 02-093 Warsaw, Poland ‡Faculty of Chemistry, Adam Mickiewicz University, Uniwersytetu Poznańskiego 8, 61-614 Poznań, Poland

E-mail: krp@fuw.edu.pl; komasa@man.poznan.pl

#### Abstract

Modern spectroscopic techniques enable the determination of the spacing between rovibrational levels of  $H_2$  with a relative accuracy of approximately  $10^{-11}$ . At this extreme level of precision, subtle quantum electrodynamics (QED) effects, such as the electron self-interaction and vacuum polarization, are probed. A theoretical model aiming to achieve similar accuracy must precisely describe not only these relatively small QED effects but also the more significant contributions related to electron correlation, coupling between electronic and nuclear motion, and relativistic effects. Although the hydrogen molecule exhibits most of the phenomena found in larger molecules, it is simple enough to meet the requirements mentioned above. In this article, we report on enhancements to current capabilities of quantum mechanical calculations for the hydrogen molecule. We present a method based on exponential functions that fully captures electron correlation, or more broadly, interparticle correlation, enabling a comprehensive description of effects related to nuclear motion. Specifically, we solve the four-particle Schrödinger equation without invoking commonly used approximations such as the one-electron or the Born-Oppenheimer approximation. The only source of nonrelativistic energy error comes from the finite size of the basis set. The explicitly correlated nonadiabatic wave function used here is then employed to determine relativistic and QED effects. As a result, the dissociation energy for the lowest rovibrational levels in the electronic ground state of H<sub>2</sub> has been obtained with a relative accuracy of  $7 \cdot 10^{-10}$ , while the frequencies of intervals between these levels have been determined with sub-MHz accuracy, corresponding to a relative accuracy of  $3 \cdot 10^{-9}$ . In consequence, the discrepancies between the highest precision measurements and earlier theoretical predictions have been resolved.

### 1 Introduction

The hydrogen molecule has served as a fundamental benchmark for theoretical calculations since the advent of quantum mechanics a hundred years ago. In 1927, Heitler and London provided the first qualitative explanation of molecular binding based on quantum mechanical principles. A few years later, James and Coolidge<sup>2</sup> reached an agreement with the then-available experimental data using an explicitly correlated wave function. Early calculations, including those by Kołos and Roothaan, were based on the clamped nuclei approximation. Efforts to incorporate nuclear motion began with the evaluation of adiabatic and nonadiabatic corrections, initiated by Kołos and Wolniewicz in the early 1960s. 4-6 The most accurate calculations of these corrections to date have been performed within the framework of nonadiabatic perturbation theory (NAPT), employing explicitly correlated exponential wave functions and expanding the perturbational series up to second order in the electron-to-nucleus mass ratio.<sup>8</sup> The first direct nonadiabatic calculation of molecular energy, bypassing the intermediate step of evaluating internuclear potentials, is also attributed to Kołos and Wolniewicz, who used a product of their electronic wave function and a harmonic oscillator nuclear function. 9 A breakthrough in accurate direct nonadiabatic calculations of the nonrelativistic component of the ground-state energy was achieved by Adamowicz and coworkers, <sup>10</sup> who employed explicitly correlated Gaussian (ECG) functions, reaching the relative accuracy of  $7 \cdot 10^{-9}$ . The accuracy was later improved to  $3 \cdot 10^{-11}$  by Puchalski et al., 11 also using ECGs. Currently, the most precise direct nonadiabatic results are obtained with exponential-type wave functions, yielding the nonrelativistic dissociation energy with an accuracy of  $10^{-8}$  cm<sup>-1</sup>, corresponding to the relative precision of  $10^{-13}$ . 12

In parallel with studies on the coupling of nuclear and electronic motion, attempts were made to estimate the contribution of relativistic effects to the energy of the hydrogen molecule. In 1961, Kołos and Wolniewicz published a pioneering work<sup>4</sup> that provided the first estimation of these relativistic effects within the framework of the Born–Oppenheimer (BO) approximation. Relativistic calculations were not pursued until 1993, when Wolniewicz

presented ground-state relativistic energies augmented by approximate QED corrections. <sup>13</sup> A significant advancement occurred in 2009 with the introduction of explicitly correlated Gaussian (ECG) functions for evaluating relativistic matrix elements, which enabled accurate determination of the dissociation energy, including the complete leading-order quantum electrodynamic (QED) correction. <sup>14,15</sup> The development of the so-called rECG functions, incorporating the cusp  $1 + r_{12}/2$  prefactor, facilitated efficient quadrature of nonstandard two-center integrals <sup>16</sup> and enabled evaluation of the higher-order QED correction potential. Subsequent studies addressed finite nuclear mass relativistic corrections using NAPT, leading to the derivation of the relativistic recoil potential, <sup>17</sup> followed by improvements in the numerical accuracy of the QED correction components. <sup>18</sup>

A fully nonadiabatic treatment of the recoil effect in the relativistic correction for H<sub>2</sub>, incorporating finite nuclear mass terms directly into the relativistic operators, was first rigorously implemented in 2018. <sup>11,19</sup> The complete expression for the leading nonadiabatic QED correction was subsequently introduced in 2019. <sup>11</sup> Nonetheless, the numerical evaluation of both types of corrections remained confined to the ground rovibrational state.

A more detailed account of the centennial history behind the effort to determine the precise total energy of the hydrogen molecule can be found in the review [20]. A key aspect of this theoretical research has been the ongoing interaction with experimental results. Over the years, the fruitful interplay between theory and experiment has led to increased precision in both fields. Of particular interest are measurable separations between energy levels, including the dissociation energy. Thanks to the long lifetimes of rovibrational states, counted in days, <sup>21</sup> H<sub>2</sub> is an attractive subject for highly precise spectroscopic measurements. The highly accurate rovibrational ladder of energy levels and the infrared (IR) spectrum of the hydrogen molecule are widely utilized across various disciplines, including astronomy, <sup>22–26</sup> plasma physics, <sup>27</sup> physical chemistry, <sup>28,29</sup> and metrology. <sup>30,31</sup>

Throughout a century of research on the hydrogen molecule, the agreement between theory and experiment has undergone continuous, albeit diminishing, fluctuations. For instance, just a decade ago, the theoretical predictions and measurements of the energy of rovibrational transitions in  $H_2$  isotopologues agreed to within 10 MHz ( $\approx 0.000\,33\,\mathrm{cm^{-1}}$ ).  $^{32-52}$  This precision opened the possibility for testing QED effects on rotational transitions,  $^{53}$  setting bounds on a hypothetical fifth force,  $^{54}$  and on the number of extra spatial dimensions.  $^{55,56}$  However, recent advancements in spectroscopic techniques have enabled measurements to achieve an accuracy of the order of 10 kHz.  $^{57-73}$  As a result, discrepancies between theory and experiment at the level of several megahertz have been revealed. It was suspected that the incomplete treatment of relativistic and QED recoil effects could be the main reason for these discrepancies.

In this article, we report the results of our calculations, which were performed using a nonadiabatic exponential wave function. Such functions possess correct asymptotic properties, but are extremely rarely used in molecular calculations due to difficulties in evaluating corresponding integrals. We have overcome these difficulties <sup>74,75</sup> and developed a method applicable to arbitrary rovibrational excitation levels of diatomic two-electron molecules, like H<sub>2</sub>, HeH<sup>+</sup>, and their isotopologues. <sup>12,76–78</sup> We also present results from using the direct nonadiabatic method to estimate relativistic and QED corrections. With this approach, we were able to bring the theoretical predictions back into agreement with the measurements at a new sub-MHz level of accuracy.

## 2 Theoretical background

Our calculations are based on the nonrelativistic quantum electrodynamic (NRQED) theory, which describes the energy of a bound rovibrational level of a light molecule as a function of the fine-structure constant  $\alpha$ . This energy can be expanded in powers of  $\alpha$  and its logarithm (atomic units are used throughout this section)

$$E(\alpha) = m \alpha^{2} E^{(2)} + m \alpha^{4} E^{(4)} + m \alpha^{4} E_{fs}^{(4)} + m \alpha^{5} E^{(5)} + m \alpha^{6} E^{(6)} + m \alpha^{7} E^{(7)} + \dots$$
 (1)

Subsequent terms of this expansion can be identified as the nonrelativistic energy, the relativistic correction, the finite nuclear size correction, the QED correction, and higher-order corrections. An important feature of NRQED is that the coefficients  $E^{(n)}$  of this expansion can be expressed as expectation values of some effective Hamiltonians  $H^{(n)}$  with the nonrelativistic wave function  $\Psi$ . These expectation values can be evaluated using a fully four-body wave function or, if this is infeasible, using approximations that involve the separation of nuclear and electronic variables, as in e.g., NAPT. Obviously, the former approach, referred to as the *direct nonadiabatic* method, is preferable because it fully accounts for the effects of the finite nuclear mass.

#### 2.1 The wave function

The wave function must reflect the rotational and electronic degrees of freedom present in the ground electronic state  $(^{1}\Sigma_{g}^{+})$  of the hydrogen molecule.  $\Psi$  should also account for the coupling between the rotational angular momentum of nuclei and orbital angular momentum of electrons  $\vec{L}$ . This coupling results in the total spatial angular momentum, represented by  $\vec{J}$ . Considering these factors, we can construct the wave function  $\Psi$  as follows:

$$\Psi^{J,M} = \sum_{\Lambda} \Psi_{\Lambda}^{J,M} \,, \tag{2}$$

where J and M are the total rotational and magnetic quantum numbers, respectively. The latter is the projection of  $\vec{J}$  onto the laboratory frame's Z axis. The summation index  $\Lambda$  is an eigenvalue of the projection of  $\vec{L}$  on the internuclear axis and runs over subsequent electronic states  $\Sigma_g, \Pi_g, \Delta_g, \ldots$ , which correspond to  $|\Lambda| = 0, 1, 2, \ldots$ 

The functions  $\Psi_{\Lambda}^{J,M}$  are represented as the linear combination

$$\Psi_{\Lambda}^{J,M} = \sum_{\{k\}} c_{\{k\}} (1 + \mathcal{P}_{12}) \, \psi_{\{k\},\Lambda}^{J,M} \tag{3}$$

of four-particle basis functions

$$\psi_{\{k\},\Lambda}^{J,M} = \mathcal{Q}_{\Lambda} e^{-\alpha_{\Lambda}R - \beta_{\Lambda}(\zeta_1 + \zeta_2)} R^{k_0} r_{12}^{k_1} \eta_1^{k_2} \eta_2^{k_3} \zeta_1^{k_4} \zeta_2^{k_5}$$
(4)

with elliptic-like coordinates  $\zeta_1 = r_{13} + r_{14}$ ,  $\eta_1 = r_{13} - r_{14}$ ,  $\zeta_2 = r_{23} + r_{24}$ ,  $\eta_2 = r_{23} - r_{24}$ , and  $\vec{R} = \vec{r}_{34}$ . From this point onward, indices 1 and 2 assigned to the distance between particles r, and later also to the particle momentum  $\vec{p}$  and mass m, will refer to the electrons, while indices 3 and 4 will correspond to protons. The exponents  $k_i$  are non-negative integers collectively denoted as  $\{k\}$ . The basis function is symmetric with respect to the inversion when  $k_2 + k_3$  is even and antisymmetric when this sum is odd. The operator  $\mathcal{P}_{12}$  permutes electrons, while the factor  $\mathcal{Q}_{\Lambda}$  determines the electronic angular momentum associated with a given basis function. Explicit expressions for  $\mathcal{Q}_{\Lambda}$  corresponding to the lowest angular momentum values are provided below:

$$Q_{\Sigma} = \mathcal{Y}_J^M \qquad \text{for } J \ge 0 \,, \tag{5}$$

$$Q_{\Pi} = \sqrt{\frac{2}{J(J+1)}} \, \rho^i \, R\left(\nabla_R^i \, \mathcal{Y}_J^M\right) \qquad \text{for } J \ge 1 \,, \tag{6}$$

$$Q_{\Delta} = \sqrt{\frac{4}{(J-1)J(J+1)(J+2)}}$$

$$\times \frac{1}{2} \left( \rho^{i} \rho'^{j} + \rho^{j} \rho'^{i} - \delta_{\perp}^{ij} \vec{\rho} \cdot \vec{\rho}' \right)$$

$$\times R^{2} \left( \nabla_{R}^{i} \nabla_{R}^{j} \mathcal{Y}_{J}^{M} \right) \quad \text{for } J \geq 2.$$

$$(7)$$

In addition to a J-dependent normalization constant, the  $\mathcal{Q}_{\Lambda}$  consists of the electronic and the nuclear parts. The electronic part is constructed from combinations of the vectors  $\vec{\rho} \equiv \vec{\rho}_a$  (a=1 or 2), which correspond to the components of the electron-nucleus vectors  $\vec{r}_{a3}$  that are perpendicular to the molecular axis. These components are defined as  $\rho_a^i = (\delta^{ij} - n^i n^j) \ r_{a3}^j$ , where  $\vec{n} = \vec{R}/R$  denotes the normalized internuclear vector. In this context, we utilize the Einstein summation convention. The nuclear part, in turn, involves derivatives with respect to nuclear coordinates of the solid harmonic  $\mathcal{Y}_J^M(\vec{n})$ .

The basis function described in Eq. (4) is referred to as the *nonadiabatic James-Coolidge* (naJC) function. This name reflects its similarity to the classic two-electron function introduced initially by James and Coolidge.<sup>2</sup> Their inspiration came from Hylleraas' function, which was designed for the helium atom in 1929.<sup>79</sup>

The nonlinear  $(\alpha_{\Lambda}, \beta_{\Lambda})$  and linear  $c_{\{k\}}$  parameters are determined variationally by solving the four-body Schrödinger equation  $H^{(2)}\Psi^{J,M} = E^{(2)}\Psi^{J,M}$  with the nonrelativistic Hamiltonian

$$H^{(2)} = T + V, (8)$$

$$T = \sum_{a=1}^{4} \frac{m}{2 \, m_a} p_a^2 \,, \tag{9}$$

$$V = \frac{1}{r_{12}} - \frac{1}{r_{13}} - \frac{1}{r_{23}} - \frac{1}{r_{14}} - \frac{1}{r_{24}} + \frac{1}{r_{34}}.$$
 (10)

According to the notation introduced earlier, for  $H_2$ ,  $m_1 = m_2 = m$  is the electron mass, and  $m_3 = m_4 = m_p$  denotes the mass of the proton. A more detailed description of the Ansatz and the results of nonrelativistic calculations performed using this wave function can be found in Refs. 74 and 12. At this point, we merely note that the nonrelativistic energy can be determined with an accuracy limited only by the uncertainties in physical constants, such as the proton-to-electron mass ratio and the Rydberg constant.

The nonrelativistic wave function described above is utilized to calculate the expectation values of operators present in the relativistic and QED Hamiltonians  $H^{(n)}$ . Relevant formulas are provided in the following subsections.

### 2.2 Relativistic correction, $E^{(4)}$

The relativistic correction is evaluated as an expectation value of the spin-independent Breit-Pauli Hamiltonian  $H^{(4)}$ . It consists of the mass velocity term, the Breit orbit-orbit terms, and the Dirac delta terms

$$E^{(4)} = -\left\langle \Psi \left| \sum_{a=1}^{4} \frac{m^{3}}{8 m_{a}^{3}} p_{a}^{4} \right| \Psi \right\rangle$$

$$- \frac{1}{2} \left\langle \Psi \left| \sum_{a=1}^{3} \sum_{b=a+1}^{4} \frac{m^{2} s_{a,b}}{m_{a} m_{b}} p_{a}^{i} \left( \frac{\delta^{ij}}{r_{ab}} + \frac{r_{ab}^{i} r_{ab}^{j}}{r_{ab}^{3}} \right) p_{b}^{j} \right| \Psi \right\rangle$$

$$- \pi \left\langle \Psi \left| \delta^{3}(r_{12}) \right| \Psi \right\rangle + \frac{\pi}{2} \left( 1 + \frac{m^{2}}{m_{p}^{2}} \right) \left\langle \Psi \left| \sum_{a=1}^{2} \sum_{b=3}^{4} \delta^{3}(r_{ab}) \right| \Psi \right\rangle. \tag{11}$$

In the above,  $s_{a,b} = 2 \left[ \delta_{a,1} \cdot \delta_{b,2} + \delta_{a,3} \cdot \delta_{b,4} \right] - 1$  provides a proper sign. To achieve the target of sub-MHz accuracy, it is essential to consider another small relativistic effect arising from the spatial distribution of the proton's charge. The leading correction due to the finite nuclear size, which is formally of the order of  $\alpha^4$ , is given by  $^{80}$ 

$$E_{\rm fs}^{(4)} = \frac{2\pi}{3} \left\langle \Psi \left| \sum_{a,X} \delta^3(r_{aX}) \right| \Psi \right\rangle \frac{r_p^2}{\tilde{\chi}^2}, \tag{12}$$

where  $r_p$  is the root mean square charge radius of the proton and  $\lambda$  is the reduced electron Compton wavelength. All the expectation values mentioned above were calculated using the naJC wave function. Detailed information regarding the newly developed integration methods, which are suitable for evaluating these expectation values, along with their regularization and numerical convergence, can be found in Refs. 75 and 81. Preliminary results for the lowest rotational levels of  $H_2$  are also shown therein.

In Eq. (11), the nucleus-nucleus Dirac delta interaction is omitted due to its negligible value. Contributions from the coupling between the nuclear spin and rotation, as well as between nuclear spins, are small because they depend quadratically on the electron-to-nucleus mass ratio. These effects are usually undetectable in infrared spectroscopy. Nonetheless, they were measured by Ramsey in 1971, 82 which allowed us, using the four-body Gaussian wave function, to determine the quadrupole moment of the deuteron to an accuracy better than for any other element of the periodic table. 30 In this work, the energy levels are averaged over the nuclear spin orientations; therefore, no hyperfine coupling is considered.

### 2.3 QED correction, $E^{(5)}$

The next term of the  $\alpha$ -expansion (1) is the leading spin-independent quantum electrodynamic correction represented by the following expression, including terms up to the first order in the electron-to-nucleus mass ratio<sup>11</sup>

$$E^{(5)} = -\frac{2}{3\pi} \frac{m^2}{\mu^2} \mathcal{D} \ln k_0$$

$$-\frac{7}{6\pi} \left\langle \Psi \left| \frac{1}{r_{12}^3} \right| \Psi \right\rangle - \frac{7}{6\pi} \sum_{a=1}^2 \sum_{b=3}^4 \frac{m}{m_b} \left\langle \Psi \left| \frac{1}{r_{ab}^3} \right| \Psi \right\rangle$$

$$+\frac{4}{3} \sum_{a=1}^2 \sum_{b=3}^4 \left\{ \frac{19}{30} - 2 \ln \alpha + \frac{m}{m_p} \left( \frac{31}{6} - \frac{1}{2} \ln \alpha \right) \right\} \left\langle \Psi \left| \delta^3(r_{ab}) \right| \Psi \right\rangle$$

$$+ \left( \frac{164}{15} + \frac{14}{3} \ln \alpha \right) \left\langle \Psi \left| \delta^3(r_{12}) \right| \Psi \right\rangle .$$

$$(13)$$

The atomic reduced mass, defined as  $\mu = m_{\rm p} \, m / \, (m_{\rm p} + m)$ , is used in this context. Eq. (13) consists of five terms. The first term contains the so-called Bethe logarithm

$$\ln k_0 = \frac{1}{\mathcal{D}} \left\langle \Psi \left| \left( \sum_{a=1}^2 \vec{p}_a \right) (H - E) \ln \left[ 2(H - E) \right] \left( \sum_{a=1}^2 \vec{p}_a \right) \right| \Psi \right\rangle, \tag{14}$$

where

$$\mathcal{D} = 2\pi \sum_{a=1}^{2} \sum_{b=3}^{4} \left\langle \Psi \left| \delta^{3}(r_{ab}) \right| \Psi \right\rangle . \tag{15}$$

The next two expressions represent the electron-electron and electron-nucleus Araki-Sucher terms, respectively. These expectation values are defined as

$$\left\langle \Psi \left| \frac{1}{r^3} \right| \Psi \right\rangle = \lim_{\epsilon \to 0} \left[ \left\langle \Psi \left| \frac{\theta(r - \epsilon)}{r^3} \right| \Psi \right\rangle + 4\pi (\gamma + \ln \epsilon) \left\langle \Psi \left| \delta^3(r) \right| \Psi \right\rangle \right], \tag{16}$$

where the symbol  $\gamma$  denotes the Euler-Mascheroni constant, and  $\theta$  is the Heaviside function. Finally, there are two terms in Eq. (13) that involve electron-electron and electron-nucleus Dirac deltas. Currently, only these two numerically dominant terms have been evaluated using the four-body naJC wave function. The remaining three terms of Eq. (13) were estimated within the framework of the BO approximation, which significantly influenced the overall error budget. The Bethe logarithm and the electron-electron Araki-Sucher BO potentials were taken from Ref. 18, while the electron-nucleus Araki-Sucher potential is from Ref. 83.

### 2.4 Higher-order QED correction, $E^{(6)}$

The higher-order QED contribution, denoted as  $E^{(6,0)}$ , is calculated within the BO approximation, using the wave function  $\Psi(\vec{r}, \vec{R}) = \phi(\vec{r}) \chi(\vec{R})$ . The energy  $E^{(6,0)}$  is expressed in terms of two internuclear potentials: the Breit-Pauli potential  $\mathcal{E}^{(4,0)}(R)$  and the higher-order relativistic potential  $\mathcal{E}^{(6,0)}(R)$ , which are defined as follows <sup>16</sup>

$$\mathcal{E}^{(4,0)}(R) = \left\langle \phi \left| H^{(4,0)} \right| \phi \right\rangle_{\text{el}}, \tag{17}$$

$$\mathcal{E}^{(6,0)}(R) = \left\langle \phi \left| H^{(6,0)} \right| \phi \right\rangle_{\text{el}} + \left\langle \phi \left| H^{(4,0)} \frac{1}{(\mathcal{E}_{\text{el}} - H_{\text{el}})'} H^{(4,0)} \right| \phi \right\rangle_{\text{el}}.$$
 (18)

The Hamiltonians  $H^{(4,0)}$  and  $H^{(6,0)}$  are the leading and higher-order relativistic Hamiltonians, respectively, both in the nonrecoil limit indicated by 0 in the superscript. This limit entails neglecting all terms that depend on nuclear mass. The expectation value symbol  $\langle \dots \rangle_{\rm el}$  means integration over electronic variables only.  $H_{\rm el} \equiv H^{(2,0)}$  and  $H_{\rm n}$  represent the electronic and nuclear components of the nonrelativistic Hamiltonian  $H^{(2)}$ , respectively. The explicit formulas for  $\mathcal{E}^{(6,0)}(R)$  are too extensive to be presented here—they can be found in Ref. 16. The total correction is obtained by integration over the nuclear variables

$$E^{(6,0)} = \left\langle \chi_{vJ} \left| \mathcal{E}^{(6,0)}(R) \right| \chi_{vJ} \right\rangle + \left\langle \chi_{vJ} \left| \mathcal{E}^{(4,0)}(R) \frac{1}{(E_{vJ}^{(2,0)} - H_{n})'} \mathcal{E}^{(4,0)}(R) \right| \chi_{vJ} \right\rangle,$$
(19)

where  $\chi$  is the nuclear wave function obtained by solving the radial Schrödinger equation. More details on how to evaluate this correction can be found in the original article. <sup>16</sup>

### 2.5 Estimation of $E^{(7)}$

The  $E^{(7)}$  term is a particularly problematic correction because its complete form is still unknown. It is therefore estimated by a dominating term inferred from the atomic hydrogen theory <sup>80</sup>

$$E^{(7)} \approx \pi \left\langle \Psi \left| \sum_{a=1}^{2} \sum_{b=3}^{4} \delta^{3}(r_{ab}) \right| \Psi \right\rangle \left\{ \frac{1}{\pi} \left[ A_{60} + A_{61} \ln \alpha^{-2} + A_{62} \ln^{2} \alpha^{-2} \right] + \frac{1}{\pi^{2}} B_{50} + \frac{1}{\pi^{3}} C_{40} \right\}.$$
(20)

This approximation adds another significant contribution to the error budget.

#### 2.6 Atomic limits

This section provides a comprehensive list of atomic thresholds relevant to the subsequent terms of Eq. (1). These atomic limits can be used in the calculation of the dissociation energy  $D_{v,J} = 2 E(H) - E(H_2)$  for a specific rovibrational level (v, J).

$$E^{(2)}(H) = -\frac{\mu}{2m},$$
 (21)

$$E^{(4)}(H) = -\frac{\mu^3}{8 m^3} \left[ 1 + 3 \frac{m}{m_p} + \frac{m^2}{m_p^2} \right], \qquad (22)$$

$$E_{\rm fs}^{(4)}({\rm H}) = \frac{2\,\mu^3}{3\,m^3}\,\frac{r_p^2}{\bar{\chi}^2}\,,\tag{23}$$

$$E^{(5)}(H) = -\frac{4}{3\pi} \frac{\mu}{m} \left( \ln k_0^{H} + \ln \frac{\mu}{m} \right) + \frac{7}{6\pi} \frac{m}{m_p} 4 \ln 2$$

$$+\frac{4}{3\pi}\frac{\mu^3}{m^3}\left[\frac{19}{30} - 2\ln\alpha + \frac{m}{m_p}\left(\frac{31}{6} - \frac{1}{2}\ln\alpha\right)\right],\tag{24}$$

$$E^{(6)}(H) = -\frac{1}{16} + \left(\frac{427}{96} - 2\ln 2\right) + \left(-\frac{9\zeta(3)}{4\pi^2} - \frac{2179}{648\pi^2} + \frac{3\ln 2}{2} - \frac{10}{27}\right)$$
(25)

$$E^{(7)}(H) = \frac{\mu^3}{m^3} \left[ \frac{1}{\pi} \left( A_{60} + A_{61} \ln \alpha^{-2} + A_{62} \ln^2 \alpha^{-2} \right) + \frac{1}{\pi^2} B_{50} + \frac{1}{\pi^3} C_{40} \right].$$
 (26)

 $\zeta$  is the Riemann zeta function. The atomic Bethe logarithm is defined as follows

$$\ln k_0^{\rm H} = \frac{1}{2} \langle \vec{p}(H - E) \ln [2(H - E)] \vec{p} \rangle$$
 (27)

with the atomic nonrelativistic Hamiltonian  $H = p^2/2 - 1/r$ . The numerical value of the hydrogenic Bethe logarithm is know to a high accuracy, <sup>84</sup>  $\ln k_0^{\rm H} = 2.984\,128\,555\,765\,498$ . In the present work, Eqs. (21)-(23) were employed in molecular calculations performed using the nonadiabatic wave function. The Bethe logarithm, in turn, was evaluated in BO approximation, which means that the first term in Eqs. (13) and (24) are modified by taking the infinite nuclear mass limit. The expression  $E^{(6)}(H)$  represents the atomic limit in the BO approximation, too. Three distinct components of Eq. (25) arise from the Dirac theory, one-loop, and two-loop QED corrections, respectively. Finally, the factor  $\mu^3/m^3$  in  $E^{(7)}(H)$  reflects the usage of the Dirac delta calculated with the fully nonadiabatic molecular wave function.

### 3 Results

Numerical calculations were performed using the CODATA 2022 recommended physical constants. <sup>80</sup> Specifically, the following constants were used: the proton-to-electron mass ratio,  $m_{\rm p}/m=1836.152\,673\,426(32)$ , the inverse fine structure constant,  $1/\alpha=137.035\,999\,177(21)$ , the Rydberg constant,  $\mathcal{R}_{\infty}=109\,737.315\,681\,57(12)\,\mathrm{cm}^{-1}$ , the proton charge radius,  $r_p=0.84075(64)$  fm, the reduced electron Compton wavelength,  $\lambda=386.159\,267\,44(12)$  fm, and the speed of light in vacuum,  $c=299\,792\,458$  m s<sup>-1</sup>. To convert our numerical results from atomic units to wavenumbers we multiply the  $E^{(n)}$  by  $2\mathcal{R}_{\infty}\,\alpha^{n-2}$ , while conversion to MHz requires multiplication by  $2\cdot 10^{-4}\,\mathcal{R}_{\infty}\,c\,\alpha^{n-2}$ .

In accordance with Eq. (1), the total energy of a rovibrational level is calculated as the sum of the nonrelativistic energy and successive corrections of increasing order in  $\alpha$ , as outlined in the previous Section. The convergence of individual relativistic expectation values, evaluated within the framework of the direct nonadiabatic approach, is demonstrated in the Supporting Information tables. Expectation values involving the electron-nucleus Dirac delta, which appear in corrections  $E_{\rm fs}^{(4)}$ ,  $E^{(5)}$ , and  $E^{(7)}$ , can also be inferred from this data. Analyzing this convergence provides a foundation for estimating the uncertainties associated

with individual corrections and the total energy. Furthermore, the results presented in these tables may serve as a benchmark for other calculation methods.

### 3.1 Dissociation energy

Table 1 provides the final results of the dissociation energy  $D_{v,J}$  for the lowest vibrational (v=0,1,2) and rotational  $(J=0,\ldots,4)$  quantum numbers. In addition to the total dissociation energy, the table includes all components of  $D_{v,J}$  that pertain to subsequent terms  $E^{(n)}$  of the  $\alpha$ -expansion. Evaluating these components requires referencing the corresponding atomic limits  $E^{(n)}(H)$ , which are discussed in Sec. 2.6. The numerical values of  $E^{(n)}(H)$  are considered exact, meaning they do not affect the uncertainty of  $D_{v,J}$ .

As mentioned in the previous Section, there are three components of the leading QED correction,  $E^{(5)}$ , that were determined within the BO approximation. To enhance the precision of this correction's final value, we utilized the precise values of these components obtained for the ground level (0,0) from the direct nonadiabatic calculations with the naECG wave function. <sup>11</sup> For all levels (v, J), we applied a uniform shift to these three components based on the difference between the nonadiabatic value and the value obtained from the BO approximation. Thus, the shifted contribution to the dissociation energy from the component Q can be expressed as  $Q_{v,J}^{\rm BO} - Q_{0,0}^{\rm BO} + Q_{0,0}^{\rm naECG}$ . The total shift from all three components is approximately  $-1.1 \cdot 10^{-5}$  cm<sup>-1</sup>. Because this is a uniform shift applied to all energy levels, it does not alter the spacing between them.

The uncertainties related to  $E^{(2)}$  and  $E^{(4)}$  are purely numerical; they arise from the finite size of the naJC basis set and have a negligible influence on the overall error budget. The most considerable contributions to the uncertainty of  $D_{v,J}$  come from  $E^{(5)}$  and  $E^{(7)}$  terms. In the first case, the primary source of error is the omission of finite mass effects in the three aforementioned components. Their uncertainties were estimated as  $\left(Q_{v,J}^{\rm BO} - Q_{0,0}^{\rm BO}\right)/\mu_{\rm n}$ , where  $\mu_{\rm n} = m_{\rm p}/2$  is the nuclear reduced mass. In the latter case, the error comes from the incompleteness of the expression for  $E^{(7)}$ . In summary, the uncertainties associated with  $D_{v,J}$  are less than  $3.3 \cdot 10^{-5} \, {\rm cm}^{-1} (\approx 1 \, {\rm MHz})$ .

Table 1: Theoretically predicted dissociation energy  $D_{v,J}$  for the five lowest rotational levels in the vibrational states v=0,1,2 of  $\mathrm{H_2}$  [cm<sup>-1</sup>]. Components of  $D_{v,J}$  related to subsequent terms  $E^{(n)}$  of the  $\alpha$ -expansion (1) are also included.

Component	$D_{0,0}$	$D_{1,0}$	$D_{2,0}$
$E^{(2)}$	36 118.797 744 716 0(40)	31 957.633 674 200(20)	28 031.795 253 030(20)
$E^{(4)}$	-0.531217263(61)	-0.554783333(62)	-0.572886764(67)
$E_{\mathrm{fs}}^{(4)}$	-0.000030900(33)	-0.000027745(30)	-0.000024797(27)
$E^{(5)}$	-0.19491021(15)	-0.173629(10)	-0.153814(20)
$E^{(6)}$	-0.0020577(66)	-0.0018664(60)	-0.0016868(54)
$E^{(7)}$	0.000101(25)	0.000090(23)	0.000081(20)
Total	36 118.069 630(26)	31956.903458(26)	28031.066922(29)
Component	$D_{0,1}$	$D_{1,1}$	$D_{2,1}$
$E^{(2)}$	36 000.312 484 230(10)	31 845.060 614 420(10)	27 925.004 807 940(20)
$E^{(4)}$	-0.53380004(31)	-0.55714556(38)	-0.57502713(41)
$E_{ m fs}^{(4)} \ E^{(5)}$	-0.000030749(33)	-0.000027603(30)	-0.000024664(27)
$E^{(5)}$	-0.19388906(52)	-0.172669(11)	-0.152912(20)
$E^{(6)}$	-0.0020488(66)	-0.0018581(60)	-0.0016789(54)
$E^{(7)}$	0.000100(25)	0.000090(22)	0.000080(20)
Total	35 999.582 816(26)	31844.329004(25)	27924.275245(29)
Component	$D_{0,2}$	$D_{1,2}$	$D_{2,2}$
$E^{(2)}$	35764.429230800(10)	31 620.965 513 400(10)	27712.440655800(20)
$E^{(4)}$	-0.53890776(38)	-0.56181401(38)	-0.57925386(41)
$E_{ m fs}^{(4)} \ E^{(5)}$	-0.000030451(33)	-0.000027322(29)	-0.000024399(26)
$E^{(5)}$	-0.1918636(15)	-0.170765(12)	-0.151123(21)
$E^{(6)}$	-0.0020312(65)	-0.0018415(59)	-0.0016633(53)
$E^{(7)}$	0.000099(25)	0.000089(22)	0.000079(20)
Total	35 763.696 497(26)	31620.231155(26)	27711.708670(29)
Component	$D_{0,3}$	$D_{1,3}$	$D_{2,3}$
$E^{(2)}$	35 413.288 018 990(10)	31 287.416 511 940(20)	27396.103055210(20)
$E^{(4)}$	-0.54642754(38)	-0.56868046(38)	-0.58546271(41)
$E_{ m fs}^{(4)} \ E^{(5)}$	-0.000030009(32)	-0.000026906(29)	-0.000024007(26)
	-0.1888668(30)	-0.167948(13)	-0.148477(22)
$E^{(6)}$	-0.0020052(64)	-0.0018169(58)	-0.0016401(53)
$E^{(7)}$	0.000098(24)	0.000088(22)	0.000078(20)
Total	35412.550787(25)	31286.678128(26)	27395.367529(30)
Component	$D_{0,4}$	$D_{1,4}$	$D_{2,4}$
$E^{(2)}$	34950.015238450(20)	30 847.433 710 540(20)	26978.912007530(20)
$E^{(4)}$	-0.55619744(35)	-0.57758917(37)	-0.59350370(40)
$E_{ m fs}^{(4)} \ E^{(5)}$	-0.000029431(32)	-0.000026362(28)	-0.000023495(25)
$E^{(5)}$	-0.1849460(49)	-0.164264(15)	-0.145018(24)
$E^{(6)}$	-0.0019711(63)	-0.0017848(57)	-0.0016098(52)
$E^{(7)}$	0.000096(24)	0.000086(21)	0.000076(19)

### 3.2 Rovibrational transition energy

Establishing reliable uncertainty for a transition frequency  $\nu$  is challenging due to the partial error cancellation between two rovibrational levels. The overall uncertainty u is calculated as the root-mean-square of the individual uncertainties  $u^{(n)}$ , which arise from the terms  $\nu^{(n)} = \Delta E^{(n)}$  in the  $\alpha$ -expansion. To determine the  $u^{(n)}$  values, we have applied distinct approaches depending on how each  $\nu^{(n)}$  term was evaluated. For  $\nu^{(n)}$  obtained with the direct nonadiabatic approach (as  $\nu^{(2)}$  and  $\nu^{(4)}$ ), the uncertainty was estimated as a maximum uncertainty of both levels. In contrast, for  $\nu^{(n)}$  calculated using the BO approximation (as  $\nu^{(5)}$  and  $\nu^{(6)}$ ), the uncertainty was estimated by the formula  $\nu^{(n)}/\mu_n$ . This scaling accounts for the missing finite nuclear mass effects. Since the complete  $\nu^{(7)}$  is currently unknown, and its dominant term from the atomic hydrogen theory only provides an estimate, we assumed a conservative error margin of 25% for this contribution. The uncertainty of  $\nu^{(4)}_{\rm fs}$  is determined by that of the proton charge radius and is relatively small compared to the main error components.

Having determined the uncertainties, we are now in a position to compare our results with experimental values — a crucial step in validating the accuracy and reliability of the theoretical model. Among the numerous rovibrational intervals measured for  $H_2$ , only nine are known with sub-MHz precision. These measurements, taken within the last two years,  $^{69-71,73,85}$  encompass both purely rotational transitions and those belonging to the fundamental vibrational band as well as the first overtone band. Table 2 presents a compilation of these experimental frequencies alongside their theoretical counterparts. Each panel in the table is dedicated to a specific transition line and includes all components that contribute to the final theoretical frequency, along with their individual error bars. The bottom row of each panel displays the difference between the theoretical and experimental frequencies, accompanied by the combined uncertainty,  $\sigma$ . We observe agreement for all nine lines, with the largest difference being  $1.4 \sigma$  for the  $Q_1(1)$  line. Figure 1 illustrates these differences relative to the  $\pm 1$  MHz band, clearly demonstrating that the theoretical predictions and spectroscopic

measurements are in sub-MHz agreement. In some cases, the experimental results are an order of magnitude more accurate than the theoretical predictions, which highlights the need for further development of computational methods, particularly for  $\nu^{(7)}$ .

Table 2: Comparison of theoretically predicted transition frequencies (in MHz) for H<sub>2</sub> with nine experimental results that were measured with sub-MHz accuracy. The components  $\nu^{(n)} = \Delta E^{(n)}$  of the theoretical frequency, corresponding to subsequent terms of the  $\alpha$ -expansion (1), are also included. CODATA 2022 recommended physical constants were used.<sup>80</sup>

Component	$S_0(0): (0,2) \to (0,0)$	$S_0(1): (0,3) \to (0,1)$	$Q_1(1): (1,1) \to (0,1)$
$\frac{1}{ u^{(2)}}$	10623700.7825(3)	17 598 550.7339(4)	124 571 317.1657(4)
$ u^{(4)}$	230.555(11)	378.562(11)	699.881(11)
$ u^{(5)}$	-91.335(47)	-150.565(77)	-636.16(33)
$ u^{(6)}$	-0.793(3)	-1.308(4)	-5.719(18)
$ u^{(7)}$	0.040(10)	0.070(17)	0.310(78)
$ u_{ m fs}^{(4)}$	-0.01346(2)	-0.02219(3)	-0.0943(1)
Theory	10623839.229(49)	17598777.469(80)	124571375.38(34)
Experiment	$10623839.09(39)^a$	$17598777.46(75)^a$	$124571374.73(31)^b$
Difference	0.14(39)	0.01(75)	0.65(46)
Component	$S_1(0): (1,2) \to (0,0)$	$Q_2(1): (2,1) \to (0,1)$	$Q_2(2): (2,2) \to (0,2)$
$ u^{(2)} $	134841618.0297(4)	242091633.7378(5)	241 392 544.6686(5)
$ u^{(4)}$	917.267(11)	1235.957(12)	1209.546(12)
$ u^{(5)}$	-723.86(37)	-1228.46(63)	-1221.38(63)
$ u^{(6)}$	-6.482(21)	-11.089(36)	-11.031(35)
$ u^{(7)}$	0.340(85)	0.59(15)	0.59(15)
$ u_{ m fs}^{(4)}$	-0.1072(2)	-0.1824(3)	-0.1814(3)
Theory	134841805.19(38)	242091630.55(65)	241392522.22(65)
Experiment	$134841805.102(15)^c$	$242091630.140(9)^d$	$241392522.00(34)^a$
Difference	0.09(38)	0.41(65)	0.22(73)
	$Q_2(3): (2,3) \to (0,3)$	$S_2(0): (2,2) \to (0,0)$	$S_2(1): (2,3) \to (0,1)$
$ u^{(2)} $	240 349 158.6533(5)	252 016 245.4511(5)	257 947 709.3872(5)
$ u^{(4)}$	1170.245(12)	1440.101(12)	1548.807(12)
$ u^{(5)}$	-1210.85(62)	-1312.71(68)	-1361.42(70)
$ u^{(6)}$	-10.945(35)	-11.824(38)	-12.253(39)
$ u^{(7)}$	0.59(15)	0.63(16)	0.66(17)
$ u_{ m fs}^{(4)}$	-0.1799(3)	-0.1949(3)	-0.2021(3)
Theory	240 349 107.52(64)	252016361.45(69)	257947884.98(72)
Experiment	$240349107.15(71)^a$	$252016361.164(8)^e$	$257947884.597(30)^a$
Difference	0.36(96)	0.28(69)	0.39(72)

<sup>&</sup>lt;sup>a</sup>Fleurbaey et al., 2023; <sup>69</sup> <sup>b</sup>Lamperti et al., 2023; <sup>70</sup> <sup>c</sup>Stankiewicz et al., 2025; <sup>73</sup> <sup>d</sup>Diouf et al., 2024; <sup>85</sup> <sup>e</sup>Cozijn et al., 2023; <sup>71</sup>

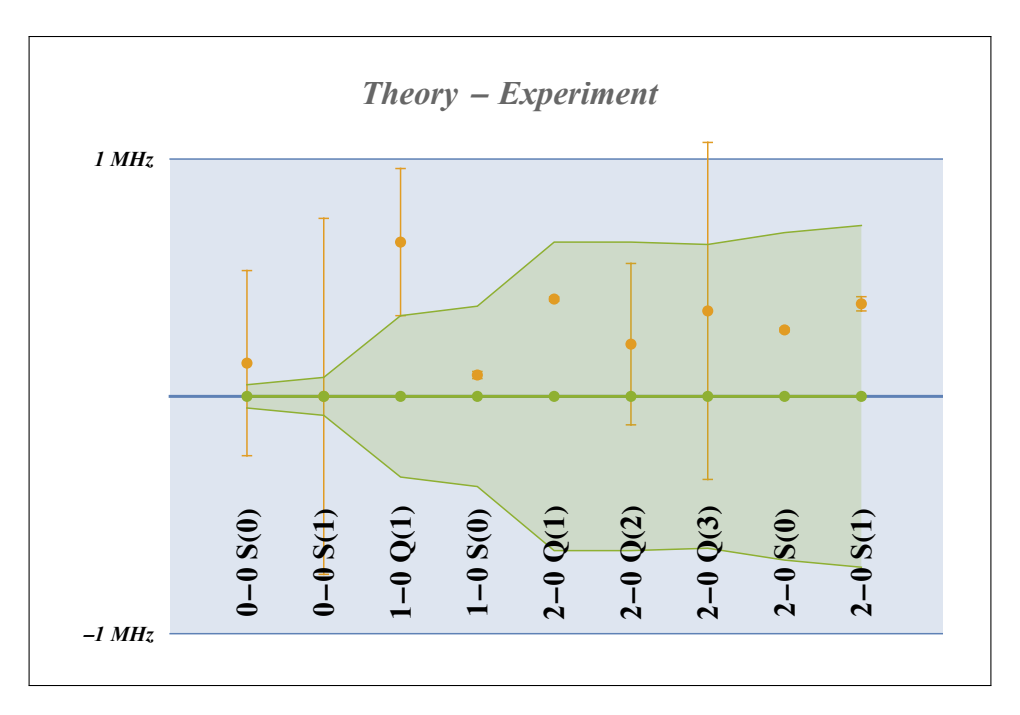


Figure 1: Differences between theoretically predicted and experimental line positions shown against the  $\pm 1$  MHz error band (in blue) and the theoretical error band (in green). The error bars around the dots come from the experiment.

Unlike earlier calculations<sup>86</sup> that estimated the relativistic and quantum electrodynamic corrections using the Born-Oppenheimer approximation, the current direct nonadiabatic results include the finite nuclear mass effects in both the relativistic and QED corrections. For frequencies in the first overtone the difference between current and previous calculations reaches 3 MHz, in the fundamental band it is approximately 1.5 MHz, and for purely rotational transitions it is about 0.1 MHz. The small third value demonstrates effective cancellation of recoil effects within a single oscillation band. The change in the total recoil effect is primarily due to relativistic and the leading QED components of the frequency.

In addition to the nine transition frequencies listed in Table 2, other energy gaps of interest for future measurements can be evaluated by calculating the difference of dissociation energies from Table 1. An upper bound for the uncertainty associated with these transitions can be inferred from Table 2: 0.1 MHz for rotational transitions, 0.4 MHz for the fundamental band, and 0.8 MHz for the first overtone. The energies for both the levels and transitions will be included in the new release of the publicly accessible H2Spectre program. <sup>86</sup>

### 4 Conclusion

We have shown that the relative uncertainty of the theoretically predicted rovibrational intervals in H<sub>2</sub> is about three parts per billion. This indicates that the calculated vibrational transition frequencies have an uncertainty at the tenth significant figure. The results obtained demonstrate that finite nuclear mass effects significantly impact not only nonrelativistic energy but also relativistic and QED corrections. By incorporating these effects, the theoretical predictions matched the experimental results with sub-MHz accuracy.

Attaining the current level of experimental accuracy is essential for testing QED within molecular systems, as well as for interpreting any discrepancies in terms of hypothetical unknown forces. There are only a few instances of physical systems where such a level of agreement between molecular or atomic spectroscopy and first-principles calculations has been achieved. Examples include the transitions in hydrogen <sup>87,88</sup> and helium atoms, <sup>89</sup> as well as those in the hydrogen molecular ion. <sup>90</sup>

Further advancements will require a fully nonadiabatic calculation of the Bethe logarithm and Araki-Sucher correction for excited rovibrational levels. We believe this task is feasible since it has already been accomplished at the ground rovibrational level.<sup>11</sup>

### Acknowledgements

This research was supported by the National Science Center (Poland) Grant No. 2021/41/B/ST4/00089.

A computer grant from the Poznań Supercomputing and Networking Center was used to carry out the numerical calculations.

### Supporting Information Available

The following files are available free of charge.

Supporting Information.pdf: Convergence of relativistic expectation values for individual rovibrational levels of H<sub>2</sub>.

### References

- (1) Heitler, W.; London, F. Wechselwirkung neutraler Atome und homeopolare Bindung nach der Quantenmechanik. Z. Phys. 1927, 44, 455.
- (2) James, H. M.; Coolidge, A. S. The Ground State of the Hydrogen Molecule. J. Chem. Phys. 1933, 1, 825.
- (3) Kolos, W.; Roothaan, C. C. J. Accurate Electronic Wave Functions for the H<sub>2</sub> Molecule. Rev. Mod. Phys. 1960, 32, 219–232.
- (4) Kołos, W.; Wolniewicz, L. The coupling between electronic and nuclear motion and the relativistic effects in the ground state of the H<sub>2</sub> molecule. Acta Phys. Pol. 1961, 20, 129–140.
- (5) Kołos, W.; Wolniewicz, L. Accurate Adiabatic Treatment of the Ground State of the Hydrogen Molecule. J. Chem. Phys. 1964, 41, 3663–3673.
- (6) Kołos, W.; Wolniewicz, L. Accurate Computation of Vibronic Energies and of Some Expectation Values for H<sub>2</sub>, D<sub>2</sub>, and T<sub>2</sub>. J. Chem. Phys. **1964**, 41, 3674.
- (7) Pachucki, K.; Komasa, J. Nonadiabatic corrections to rovibrational levels of H<sub>2</sub>. *J. Chem. Phys.* **2009**, *130*, 164113.
- (8) Pachucki, K.; Komasa, J. Leading order nonadiabatic corrections to rovibrational levels of H<sub>2</sub>, D<sub>2</sub>, and T<sub>2</sub>. J. Chem. Phys. **2015**, 143, 034111.
- (9) Kołos, W.; Wolniewicz, L. Nonadiabatic Theory for Diatomic Molecules and Its Application to the Hydrogen Molecule. *Rev. Mod. Phys.* **1963**, *35*, 473.
- (10) Kinghorn, D. B.; Adamowicz, L. Improved Nonadiabatic Ground-State Energy Upper Bound for Dihydrogen. *Phys. Rev. Lett.* **1999**, *83*, 2541–2543.

- (11) Puchalski, M.; Komasa, J.; Czachorowski, P.; Pachucki, K. Nonadiabatic QED Correction to the Dissociation Energy of the Hydrogen Molecule. *Phys. Rev. Lett.* 2019, 122, 103003.
- (12) Pachucki, K.; Komasa, J. Nonadiabatic rotational states of the hydrogen molecule. *Phys. Chem. Chem. Phys.* **2018**, *20*, 247–255.
- (13) Wolniewicz, L. Relativistic energies of the ground state of the hydrogen molecule. *J. Chem. Phys.* **1993**, *99*, 1851.
- (14) Piszczatowski, K.; Lach, G.; Przybytek, M.; Komasa, J.; Pachucki, K.; Jeziorski, B. Theoretical Determination of the Dissociation Energy of Molecular Hydrogen. J. Chem. Theory Comput. 2009, 5, 3039.
- (15) Komasa, J.; Piszczatowski, K.; Łach, G.; Przybytek, M.; Jeziorski, B.; Pachucki, K. Quantum Electrodynamics Effects in Rovibrational Spectra of Molecular Hydrogen. J. Chem. Theory Comput. 2011, 7, 3105–3115.
- (16) Puchalski, M.; Komasa, J.; Czachorowski, P.; Pachucki, K. Complete  $\alpha^6$  m Corrections to the Ground State of H<sub>2</sub>. Phys. Rev. Lett. **2016**, 117, 263002.
- (17) Czachorowski, P.; Puchalski, M.; Komasa, J.; Pachucki, K. Nonadiabatic relativistic correction in H<sub>2</sub>, D<sub>2</sub>, and HD. *Phys. Rev. A* **2018**, *98*, 052506.
- (18) Siłkowski, M.; Pachucki, K.; Komasa, J.; Puchalski, M. Leading-order QED effects in the ground electronic state of molecular hydrogen. *Phys. Rev. A* **2023**, *107*, 032807.
- (19) Wang, L. M.; Yan, Z.-C. Relativistic corrections to the ground state of H<sub>2</sub> calculated without using the Born-Oppenheimer approximation. *Phys. Rev. A* **2018**, *97*, 060501.
- (20) Puchalski, M.; Moszyński, R.; Komasa, J. In *Polish Quantum Chemistry from Kołos to Now*; Musiał, M., Grabowski, I., Eds.; Advances in Quantum Chemistry; Academic Press, 2023; Vol. 87; pp 1–36.

- (21) Pachucki, K.; Komasa, J. Magnetic dipole transitions in the hydrogen molecule. *Phys. Rev. A* **2011**, *83*, 032501.
- (22) Margolis, J.; Hunt, G. On the level of H<sub>2</sub> quadrupole absorption in the Jovian atmosphere. *Icarus* **1973**, *18*, 593–598.
- (23) Roueff, E.; Abgrall, H.; Czachorowski, P.; Pachucki, K.; Puchalski, M.; Komasa, J. The full infrared spectrum of molecular hydrogen. *Astron. Astrophys.* **2019**, *630*, A58.
- (24) Tchernyshyov, K. A Detection of H<sub>2</sub> in a High-velocity Cloud toward the Large Magellanic Cloud. Astrophys. J. **2022**, 931, 78.
- (25) Jacob, A. Small molecules, big impact: a tale of hydrides past, present, and future.

  Astrophys. Space Sci. 2023, 368, 76.
- (26) Tennyson et al., J. The 2024 release of the ExoMol database: Molecular line lists for exoplanet and other hot atmospheres. J. Quant. Spectrosc. Radiat. Transfer 2024, 326, 109083.
- (27) Bruno, D. Uncertainty quantification of a collisional-radiative model for hydrogen plasmas. *Phys. Scr.* **2025**, *100*, 035611.
- (28) Zúñiga, J.; Bastida, A.; Requena, A.; Cerezo, J. Ab Initio Partition Functions and Thermodynamic Quantities for the Molecular Hydrogen Isotopologues. J. Phys. Chem. A 2021, 125, 9226–9241.
- (29) Leachman, J. W.; Wilhelmsen, Ø.; Matveev, K. I. Cool Fuel: The Science and Engineering of Cryogenic Hydrogen; Oxford University Press, 2025.
- (30) Puchalski, M.; Komasa, J.; Pachucki, K. Hyperfine Structure of the First Rotational Level in H<sub>2</sub>, D<sub>2</sub> and HD Molecules and the Deuteron Quadrupole Moment. *Phys. Rev.* Lett. 2020, 125, 253001.

- (31) Puchalski, M.; Komasa, J.; Spyszkiewicz, A.; Pachucki, K. Nuclear magnetic shielding in HD and HT. *Phys. Rev. A* **2022**, *105*, 042802.
- (32) Kassi, S.; Campargue, A. Electric quadrupole and dipole transitions of the first overtone band of HD by CRDS between 1.45 and 1.33 μm. J. Mol. Spectrosc. **2011**, 267, 36.
- (33) Campargue, A.; Kassi, S.; Pachucki, K.; Komasa, J. The absorption spectrum of H<sub>2</sub>: CRDS measurements of the (2-0) band, review of the literature data and accurate ab initio line list up to 35000 cm<sup>-1</sup>. Phys. Chem. Chem. Phys. **2012**, 14, 802.
- (34) Kassi, S.; Campargue, A.; Pachucki, K.; Komasa, J. The absorption spectrum of D<sub>2</sub>: Ultrasensitive cavity ring down spectroscopy of the (2-0) band near 1.7  $\mu$ m and accurate ab initio line list up to 24 000 cm<sup>-1</sup>. J. Chem. Phys. **2012**, 136, 184309.
- (35) Cheng, C.-F.; Sun, Y. R.; Pan, H.; Wang, J.; Liu, A.-W.; Campargue, A.; Hu, S.-M. Electric-quadrupole transition of H<sub>2</sub> determined to 10<sup>-9</sup> precision. *Phys. Rev. A* **2012**, 85, 024501.
- (36) Dickenson, G. D.; Niu, M. L.; Salumbides, E. J.; Komasa, J.; Eikema, K. S. E.; Pachucki, K.; Ubachs, W. Fundamental Vibration of Molecular Hydrogen. *Phys. Rev. Lett.* 2013, 110, 193601.
- (37) Niu, M.; Salumbides, E.; Dickenson, G.; Eikema, K.; Ubachs, W. Precision spectroscopy of the rovibrational splittings in H<sub>2</sub>, HD and D<sub>2</sub>. J. Mol. Spectrosc. **2014**, 300, 44 54.
- (38) Tan, Y.; Wang, J.; Cheng, C.-F.; Zhao, X.-Q.; Liu, A.-W.; Hu, S.-M. Cavity ring-down spectroscopy of the electric quadrupole transitions of in the 784-852 nm region. *J. Mol. Spectrosc.* **2014**, 300, 60 64.
- (39) Kassi, S.; Campargue, A. Electric quadrupole transitions and collision-induced absorption in the region of the first overtone band of H<sub>2</sub> near 1.25μm. Journal of Molecular Spectroscopy 2014, 300, 55–59.

- (40) Mondelain, D.; Kassi, S.; Sala, T.; Romanini, D.; Gatti, D.; Campargue, A. Sub-MHz accuracy measurement of the S(2) 2-0 transition frequency of D<sub>2</sub> by Comb-Assisted Cavity Ring Down spectroscopy. J. Mol. Spectrosc. **2016**, 326, 5 8.
- (41) Wcisło, P.; Thibault, F.; Zaborowski, M.; Wójtewicz, S.; Cygan, A.; Kowzan, G.; Masłowski, P.; Komasa, J.; Puchalski, M.; Pachucki, K.; Ciuryło, R.; Lisak, D. Accurate deuterium spectroscopy for fundamental studies. J. Quant. Spectrosc. Radiat. Transfer 2018, 213, 41 – 51.
- (42) Trivikram, T. M.; Schlösser, M.; Ubachs, W.; Salumbides, E. J. Relativistic and QED Effects in the Fundamental Vibration of T<sub>2</sub>. Phys. Rev. Lett. **2018**, 120, 163002.
- (43) Tao, L.-G.; Liu, A.-W.; Pachucki, K.; Komasa, J.; Sun, Y. R.; Wang, J.; Hu, S.-M. Toward a Determination of the Proton-Electron Mass Ratio from the Lamb-Dip Measurement of HD. Phys. Rev. Lett. 2018, 120, 153001.
- (44) Fasci, E.; Castrillo, A.; Dinesan, H.; Gravina, S.; Moretti, L.; Gianfrani, L. Precision spectroscopy of HD at 1.38 μm. *Phys. Rev. A* **2018**, *98*, 022516.
- (45) Martinez, R. Z.; Bermejo, D.; Wcisło, P.; Thibault, F. Accurate wavenumber measurements for the  $S_0(0)$ ,  $S_0(1)$ , and  $S_0(2)$  pure rotational Raman lines of D<sub>2</sub>. J. Raman Spectrosc. **2019**, 50, 127–129.
- (46) Hölsch, N.; Beyer, M.; Salumbides, E. J.; Eikema, K. S. E.; Ubachs, W.; Jungen, C.; Merkt, F. Benchmarking Theory with an Improved Measurement of the Ionization and Dissociation Energies of H<sub>2</sub>. Phys. Rev. Lett. 2019, 122, 103002.
- (47) Beyer, M.; Hölsch, N.; Hussels, J.; Cheng, C.-F.; Salumbides, E. J.; Eikema, K. S. E.; Ubachs, W.; Jungen, C.; Merkt, F. Determination of the Interval between the Ground States of Para- and Ortho-H<sub>2</sub>. Phys. Rev. Lett. 2019, 123, 163002.

- (48) Lai, K.-F.; Czachorowski, P.; Schlösser, M.; Puchalski, M.; Komasa, J.; Pachucki, K.; Ubachs, W.; Salumbides, E. J. Precision tests of nonadiabatic perturbation theory with measurements on the DT molecule. *Phys. Rev. Research* **2019**, *1*, 033124.
- (49) Lai, K.-F.; Hermann, V.; Trivikram, M.; Diouf, M.; Schlösser, M.; Ubachs, W.; Salumbides, E. Precision measurement of the fundamental vibrational frequencies of tritium-bearing hydrogen molecules: T<sub>2</sub>, DT, HT. Phys. Chem. Chem. Phys. 2020, 22, 8973–8987.
- (50) Mondelain, D.; Kassi, S.; Campargue, A. Transition frequencies in the (2-0) band of D<sub>2</sub> with MHz accuracy. J. Quant. Spectrosc. Radiat. Transfer **2020**, 253, 107020.
- (51) Jóźwiak, H.; Cybulski, H.; Wcisło, P. Hyperfine structure of quadrupole rovibrational transitions in tritium-bearing hydrogen isotopologues. J. Quant. Spectrosc. Radiat. Transfer 2020, 256, 107255.
- (52) Kassi, S.; Fleurbaey, H.; Campargue, A. First detection and absolute transition frequencies in the (3–0) band of D<sub>2</sub>. J. Chem. Phys. **2024**, 160, 094306.
- (53) Salumbides, E. J.; Dickenson, G. D.; Ivanov, T. I.; Ubachs, W. QED Effects in Molecules: Test on Rotational Quantum States of H<sub>2</sub>. Phys. Rev. Lett. 2011, 107, 043005.
- (54) Salumbides, E. J.; Koelemeij, J. C. J.; Komasa, J.; Pachucki, K.; Eikema, K. S. E.; Ubachs, W. Bounds on fifth forces from precision measurements on molecules. *Phys. Rev. D* 2013, 87, 112008.
- (55) Salumbides, E. J.; Schellekens, A. N.; Gato-Rivera, B.; Ubachs, W. Constraints on extra dimensions from precision molecular spectroscopy. *New J. Phys.* **2015**, *17*, 033015.
- (56) Ubachs, W.; Koelemeij, J.; Eikema, K.; Salumbides, E. Physics beyond the Standard Model from hydrogen spectroscopy. J. Mol. Spectrosc. 2016, 320, 1 12.

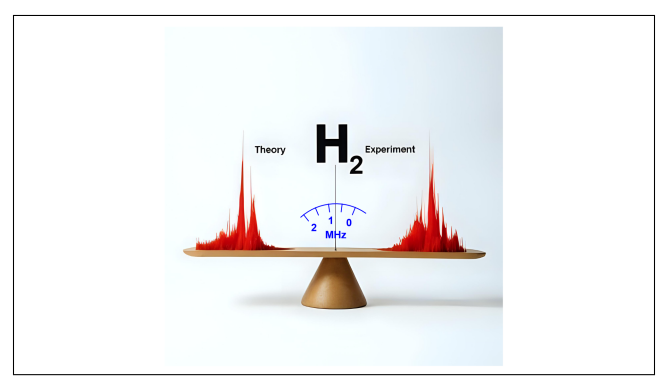
- (57) Drouin, B. J.; Yu, S.; Pearson, J. C.; Gupta, H. Terahertz spectroscopy for space applications: 2.5-2.7 THz spectra of HD, H<sub>2</sub>O and NH<sub>3</sub>. J. Mol. Spectrosc. **2011**, 1006, 2-12.
- (58) Cozijn, F. M. J.; Dupré, P.; Salumbides, E. J.; Eikema, K. S. E.; Ubachs, W. Sub-Doppler Frequency Metrology in HD for Tests of Fundamental Physics. *Phys. Rev. Lett.* 2018, 120, 153002.
- (59) Diouf, M. L.; Cozijn, F. M. J.; Darquié, B.; Salumbides, E. J.; Ubachs, W. Lamb-dips and Lamb-peaks in the saturation spectrum of HD. *Opt. Lett.* **2019**, *44*, 4733–4736.
- (60) Diouf, M. L.; Cozijn, F. M. J.; Lai, K.-F.; Salumbides, E. J.; Ubachs, W. Lamb-peak spectrum of the HD (2-0) P(1) line. Phys. Rev. Research 2020, 2, 023209.
- (61) Hua, T.-P.; Sun, Y. R.; Hu, S.-M. Dispersion-like lineshape observed in cavity-enhanced saturation spectroscopy of HD at 1.4 μm. Opt. Lett. **2020**, 45, 4863–4866.
- (62) Wójtewicz, S.; Gotti, R.; Gatti, D.; Lamperti, M.; Laporta, P.; Jóźwiak, H.; Thibault, F.; Wcisło, P.; Marangoni, M. Accurate deuterium spectroscopy and comparison with ab initio calculations. *Phys. Rev. A* **2020**, *101*, 052504.
- (63) Fast, A.; Meek, S. A. Sub-ppb Measurement of a Fundamental Band Rovibrational Transition in HD. *Phys. Rev. Lett.* **2020**, *125*, 023001.
- (64) Castrillo, A.; Fasci, E.; Gianfrani, L. Doppler-limited precision spectroscopy of HD at 1.4 μm: An improved determination of the R(1) center frequency. Phys. Rev. A 2021, 103, 022828.
- (65) Fast, A.; Meek, S. A. Precise measurement of the D<sub>2</sub> S<sub>1</sub>(0) vibrational transition frequency. *Mol. Phys.* **2022**, *120*, e1999520.
- (66) Kassi, S.; Lauzin, C.; Chaillot, J.; Campargue, A. The (2-0) R(0) and R(1) transition

- frequencies of HD determined to a  $10^{-10}$  relative accuracy by Doppler spectroscopy at 80 K. *Phys. Chem. Chem. Phys.* **2022**, 24, 23164-23172.
- (67) Cozijn, F. M. J.; Diouf, M. L.; Hermann, V.; Salumbides, E. J.; Schlösser, M.; Ubachs, W. Rotational level spacings in HD from vibrational saturation spectroscopy. *Phys. Rev. A* 2022, 105, 062823.
- (68) Cozijn, F. M. J.; Diouf, M. L.; Ubachs, W. Saturation spectroscopy of R(0), R(2) and P(2) lines in the (2-0) band of HD. Eur. Phys. J. D 2022, 76, 220.
- (69) Fleurbaey, H.; Koroleva, A. O.; Kassi, S.; Campargue, A. The high-accuracy spectroscopy of H<sub>2</sub> rovibrational transitions in the (2-0) band near 1.2 μm. Phys. Chem. Chem. Phys. 2023, 25, 14749–14756.
- (70) Lamperti, M.; Rutkowski, L.; Ronchetti, D.; Gatti, D.; Gotti, R.; Cerullo, G.; Thibault, F.; Jóźwiak, H.; Wójtewicz, S.; Masłowski, P.; Wcisło, P.; Polli, D.; Marangoni1, M. Stimulated Raman scattering metrology of molecular hydrogen. Commun. Phys. 2023, 6, 67.
- (71) Cozijn, F. M. J.; Diouf, M. L.; Ubachs, W. Lamb Dip of a Quadrupole Transition in H<sub>2</sub>. Phys. Rev. Lett. **2023**, 131, 073001.
- (72) Cozijn, F. M. J.; Diouf, M. L.; Ubachs, W.; Hermann, V.; Schlösser, M. Precision Measurement of Vibrational Quanta in Tritium Hydride. Phys. Rev. Lett. 2024, 132, 113002.
- (73) Stankiewicz, K.; Makowski, M.; Słowiński, M.; Sołtys, K. L.; Bednarski, B.; Jóźwiak, H.; Stolarczyk, N.; Narożnik, M.; Kierski, D.; Wójtewicz, S.; Cygan, A.; Kowzan, G.; Masłowski, P.; Piwiński, M.; Lisak, D.; Wcisło, P. Cavity-enhanced spectroscopy in the deep cryogenic regime new hydrogen technologies for quantum sensing. *preprint* arXiv:2502.12703 2025,

- (74) Pachucki, K.; Komasa, J. Schrödinger equation solved for the hydrogen molecule with unprecedented accuracy. *J. Chem. Phys.* **2016**, *144*, 164306.
- (75) Pachucki, K.; Komasa, J. Integrals for relativistic nonadiabatic energies of  $H_2$  in an exponential basis. *Phys. Rev. A* **2024**, *109*, 032822.
- (76) Pachucki, K.; Komasa, J. Nonrelativistic energy levels of HD. *Phys. Chem. Chem. Phys.* **2018**, *20*, 26297–26302.
- (77) Pachucki, K.; Komasa, J. Nonrelativistic energy levels of D<sub>2</sub>. Phys. Chem. Chem. Phys. **2019**, 21, 10272–10276.
- (78) Pachucki, K.; Komasa, J. Nonrelativistic energy of tritium-containing hydrogen molecule isotopologues. *Mol. Phys.* **2022**, *120*, e2040627.
- (79) Hylleraas, E. Neue Berechnung der Energie des Heliums im Grundzustande, sowie des tiefsten Terms von Ortho-Helium. Z. Physik 1929, 54, 347–366.
- (80) Mohr, P. J.; Newell, D. B.; Taylor, B. N.; Tiesinga, E. CODATA recommended values of the fundamental physical constants: 2022. Rev. Mod. Phys. 2025, 97, 025002.
- (81) Pachucki, K.; Komasa, J. Relativistic Correction from the Four-Body Nonadiabatic Exponential Wave Function. J. Chem. Theory Comput. 2024, 20, 8644–8651.
- (82) Code, R. F.; Ramsey, N. F. Molecular-Beam Magnetic Resonance Studies of HD and D<sub>2</sub>. Phys. Rev. A **1971**, 4, 1945–1959.
- (83) Pachucki, K.; Komasa, J. Electron-nucleus Araki-Sucher QED correction to rovibrational levels of H<sub>2</sub>. **2025**, in preparation.
- (84) Drake, G. W. F.; Swainson, R. A. Bethe logarithms for hydrogen up to n=20, and approximations for two-electron atoms. *Phys. Rev. A* **1990**, *41*, 1243–1246.

- (85) Diouf, M. L.; Cozijn, F. M. J.; Ubachs, W. Hyperfine structure in a vibrational quadrupole transition of ortho-H<sub>2</sub>. *Mol. Phys.* **2024**, *122*, e2304101.
- (86) H2Spectre ver. 7.4 Fortran source code 2022; https://www.fuw.edu.pl/~krp/;https://qcg.home.amu.edu.pl/H2Spectre.html.
- (87) Parthey, C. G.; Matveev, A.; Alnis, J.; Bernhardt, B.; Beyer, A.; Holzwarth, R.; Maistrou, A.; Pohl, R.; Predehl, K.; Udem, T.; Wilken, T.; Kolachevsky, N.; Abgrall, M.; Rovera, D.; Salomon, C.; Laurent, P.; Hänsch, T. W. Improved Measurement of the Hydrogen 1S-2S Transition Frequency. Phys. Rev. Lett. 2011, 107, 203001.
- (88) Pachucki, K.; Jentschura, U. D. Two-Loop Bethe-Logarithm Correction in Hydrogenlike Atoms. *Phys. Rev. Lett.* **2003**, *91*, 113005.
- (89) Clausen, G.; Scheidegger, S.; Agner, J. A.; Schmutz, H.; Merkt, F. Imaging-Assisted Single-Photon Doppler-Free Laser Spectroscopy and the Ionization Energy of Metastable Triplet Helium. *Phys. Rev. Lett.* **2023**, *131*, 103001.
- (90) Alighanbari, S.; Schenkel, M.; Korobov, V.; Schiller, S. High-accuracy laser spectroscopy of and the proton–electron mass ratio. *Nature* **2025**, *644*, 69–75.

# TOC Graphic



Al-generated base with hand-drawn augmentation